Theoretical Study of Conditions for Generation of Periodic Wellbore Flow: Dependence on Two-Phase Flow Models

Mitsuo Matsumoto[1] and Naoto Yoshida[2]

[1]Department of Earth Resources Engineering, Faculty of Engineering, Kyusyu University, Motooka 744, Nishi-ku, Fukuoka 819-0395, Japan

[2]Department of Earth Resources Engineering, Graduate School of Engineering, Kyusyu University, Motooka 744, Nishi-ku, Fukuoka 819-0395, Japan

matsumoto@mine.kyushu-u.ac.jp

Keywords: *cycling wells, two-phase flow model, slip, transient wellbore flow, numerical simulation*

ABSTRACT

The periodic flow generated in a wellbore intersecting two reservoirs was theoretically investigated by performing numerical experiments of 200 runs in total. In particular, the condition for generating periodicity, established by one of the authors using the homogeneous flow model, was validated using the slip model, which considers the slip between the liquid and vapor phases. This condition is described based on the mean specific enthalpy of the shallow and deep reservoirs weighted by their productivity indices. The inflow of the low-enthalpy fluid at the shallow feed zone triggers periodic wellbore flow.

The slip limits the upflow of the liquid phase in the wellbore and significantly affects the appearance of constant, periodic, and unstable flow patterns. Nevertheless, the results of the numerical experiments supported the generality of the condition for generating periodicity, regardless of the two-phase flow models, and its applicability to actual wells. This finding will facilitate sustaining the output of geothermal power plants by developing effective measures to stabilize the wellbore flow.

1. INTRODUCTION

Periodic changes in the wellhead pressure and flow rate, occasionally observed in production wells, pose challenges for the sustainable operation of geothermal power plants. Owing to the difficulty in directly observing periodic, often surging, wellbore flows using logging tools placed in the wellbore, numerical modeling is expected to be an effective supplementary approach to reveal the mechanism and conditions generating the periodicity. Periodic wellbore flow is generated under various conditions, such as intersecting multiple reservoirs with different fluid enthalpies and/or phase conditions (Grant et al., 1979; Grant and Bixley, 2011; Itoi et al., 2013; Iwata et al., 2002), a poorly permeable reservoir with a high-enthalpy fluid (Grant and Bixley, 2011), and fork-leg wells (Matus et al., 2020). An adequate understanding of the mechanisms and conditions for generating periodicity under each condition will facilitate sustaining the output of geothermal power plants by developing effective measures to stabilize the wellbore flow.

The authors and their colleagues investigated the mechanism under one of these conditions, a production well intersecting two reservoirs with different fluid enthalpies, using numerical modeling of transient wellbore flow (Inagaki et al., 2014; Itoi et al., 2013, 2014; Katayama et al., 2011, 2013; Matsumoto et al., 2021; Matsumoto et al., 2023; Yamamura et al., 2016, 2017). In particular, Matsumoto et al. (2021) established a universal condition for generating periodicity:

$$h_{\mathrm{L}} > \frac{\kappa \mathrm{PI_D} h_{\mathrm{reD}} + \mathrm{PI_S} h_{\mathrm{reS}}}{\kappa \mathrm{PI_D} + \mathrm{PI_S}}, \quad (1)$$

where PI and h_{re} scripted by D or S denote the productivity index and specific enthalpy of deep or shallow reservoirs, respectively; h_{L} represents the lower limit of specific enthalpy to sustain production solely from the deep reservoir; and κ represents an empirical factor. The right-hand side of Equation 1 represents the mean specific enthalpy of the fluids in the shallow and deep reservoirs, weighted by their productivity indices. The factor κ modifies the weight, depending on several conditions such as wellbore diameters, wellhead pressure, and reservoir pressure.

Equation 1 was derived from numerical experiments using an in-house wellbore flow simulator that assumed a homogeneous flow model for two-phase flow. Validation of this condition using different two-phase flow models is crucial to confirm its generality and applicability to actual geothermal wells. In this context, we designed and performed numerical experiments under the same conditions as Matsumoto et al. (2021), except that we considered the slip between the liquid and vapor phases. This study presents a partial validation using a slip model, which assumes that the slip ratio of both phases is based on an empirical equation. Future studies will employ more sophisticated models, such as drift-flux models, for two-phase flows.

We employed an extended version of the in-house simulator developed by Matsumoto et al. (2021). If other potential simulators for transient wellbore flow (e.g., Pan and Oldenburg, 2014; Tonkin et al., 2023) are employed, some modifications might be required to ensure strict energy conservation along with inflow and outflow, switching periodically between the wellbore and reservoir by overcoming numerical dispersion. Matsumoto et al. (2021) demonstrated that insufficient energy conservation at a feed zone results in non-negligible energy loss, causing the degradation of stable periodic wellbore flow.

2. MODEL DESCRIPTION

As Tonkin et al. (2021) defined, ‘static’ and ‘flowing’ mass fractions represent the ratio of the mass of a phase to the total mass of the mixture existing and flowing, respectively, in a wellbore at an instant. Using these mass fractions, we define static and flowing mean values of a variable ψ, except for density, as follows:

ISSN 2703-4275

$$\psi_{\mathrm{mix}} = \frac{\rho_{\mathrm{l}} S_{\mathrm{l}}}{\rho_{\mathrm{mix}}} \psi_{\mathrm{l}} + \frac{\rho_{\mathrm{v}} S_{\mathrm{v}}}{\rho_{\mathrm{mix}}} \psi_{\mathrm{v}}, \quad (2)$$

$$\psi_{\mathrm{f,mix}} = \frac{\rho_{\mathrm{l}} u_{\mathrm{l}} S_{\mathrm{l}}}{\rho_{\mathrm{mix}} u_{\mathrm{mix}}} \psi_{\mathrm{l}} + \frac{\rho_{\mathrm{v}} u_{\mathrm{v}} S_{\mathrm{v}}}{\rho_{\mathrm{mix}} u_{\mathrm{mix}}} \psi_{\mathrm{v}}, \quad (3)$$

where ρ, S, and u scripted by l or v denote the density, saturation (i.e., volumetric fraction), and flow velocity of liquid or vapor phases, respectively; $\rho_{\mathrm{mix}} = \rho_{\mathrm{l}} S_{\mathrm{l}} + \rho_{\mathrm{v}} S_{\mathrm{v}}$ represents the mean density of the mixture.

The two-phase transient wellbore flow of pure water can be described using three conservation equations: mass, energy, and momentum. We employ a unified form for conservation, as follows:

$$\frac{\partial}{\partial t} \rho_{\mathrm{mix}} \psi_{\mathrm{mix}} + \frac{\partial}{\partial z} \rho_{\mathrm{mix}} u_{\mathrm{mix}} \psi_{\mathrm{f,mix}} = \Psi, \quad (4)$$

where the general variable ψ is replaced with unity, specific enthalpy h, and flow velocity u, to represent mass, energy, and momentum conservation, respectively; t and z are time and drilling depth, respectively. The changes in the mechanical energy were assumed to be negligible. The right-hand side of Equation 4 Ψ, depending on the conservation equations to be considered, is replaced with the expressions presented by Matsumoto et al. (2021) to take into account the flow between the wellbore and reservoir as well as volume forces due to pressure gradient, friction, and gravity. The mass flow rate between the wellbore and reservoir varies depending on the productivity index and the pressure difference between the feed zone and reservoir. Thus, the conservation equations coincide with those of Matsumoto et al. (2021) by assuming $u_{\mathrm{mix}} = u_{\mathrm{l}} = u_{\mathrm{v}}$ (i.e., $\psi_{\mathrm{f,mix}} = \psi_{\mathrm{mix}}$) to employ the homogeneous flow model.

The slip between the liquid and vapor phases obeys the empirical equation presented by Smith (1969–70):

$$\frac{u_{\mathrm{v}}}{u_{\mathrm{l}}} = e + (1 - e) \left(\frac{\rho_{\mathrm{l}}}{\rho_{\mathrm{v}}} \right)^{\frac{1}{2}} \left(\frac{1 + e \frac{1 - x}{x} \cdot \frac{\rho_{\mathrm{v}}}{\rho_{\mathrm{l}}}}{1 + e \frac{1 - x}{x}} \right)^{\frac{1}{2}}, \quad (5)$$

where $x = \rho_{\mathrm{v}} u_{\mathrm{v}} S_{\mathrm{v}} / \rho_{\mathrm{mix}} u_{\mathrm{mix}}$ is the flowing mass fraction of the vapor phase (i.e., quality); the recommended value of the empirical constant e is 0.4. Referring to Equation 5 and the other constitutive equations included on the right-hand side of Equation 4, we can select three primary variables of pressure P, static mean flow velocity u_{mix}, and flowing mean specific enthalpy $h_{\mathrm{f,mix}}$, which sufficiently describe the state of the wellbore flow at an arbitrary time t and depth z.

By discretizing Equation 4 using the fully implicit finite difference method, we obtain a large system of nonlinear equations with respect to the primary variables at each grid point in the domain of the numerical model. The nonlinear system was iteratively solved using the Newton–Raphson method to advance each time step, which included solving a linear system using the biconjugate gradient stabilized method with the preconditioner of incomplete LU decomposition. A uniform staggered grid was used to simulate the transient wellbore flow by efficiently handling the interaction between the scalar and vector variables, whereas the steady-state flow, assumed for the initial conditions, was simulated using a uniform normal grid.

3. NUMERICAL EXPERIMENTS

The numerical experiments aimed to investigate the dependence of the wellbore flow periodicity on two-phase flow models. In particular, we focus on the validity of the condition for generating periodicity (Equation 1), which has not been investigated using two-phase flow models that assume slip between the liquid and vapor phases. By designing the same experimental conditions as those of Matsumoto et al. (2021), except for the two-phase flow models, we compared the parameter values at the boundary dividing into periodic and constant flows.

We assumed a vertical well intersecting two circular horizontal reservoirs at 1400 and 2000 m (Figure 1). The deep reservoir is placed at the bottom of the well. The inner diameter of the wellbore is uniform at 0.20 m. The frictional pressure loss in the wellbore obeys the Colebrook equation (Colebrook, 1939) with a roughness of 0.0478 mm. The shallow and deep reservoir pressures are 4.5 MPa and 10.0 MPa, respectively. Fifty runs for simulating production for 12 h were performed by assuming the temperatures and permeability–thickness products of the shallow reservoir, ranging 160–250°C and 1.0–8.0 × 10^{-12} m^3, respectively, while those of the deep reservoir were held constant at 260°C and 1.0 × 10^{-12} m^3. The productivity indices of the shallow and deep reservoirs were computed and applied to each run based on the steady-state solution of the reservoir pressure distribution with a reservoir radius of 1000 m. The wellhead pressure was maintained at 0.70 MPa. The grid size for spatial discretization was uniformly 1.0 m, while the time step size varied dynamically between 0.01 and 1.00 s, depending on requirement for successful convergence of the Newton–Raphson iteration. In addition to the reference case for the set of the aforementioned 50 runs, three variant cases were simulated with different wellbore inner diameter (0.14 m), wellhead pressure (0.30 MPa), and shallow reservoir pressure (5.0 MPa), each of which contained 50 runs. Therefore, a total of 200 runs were performed.

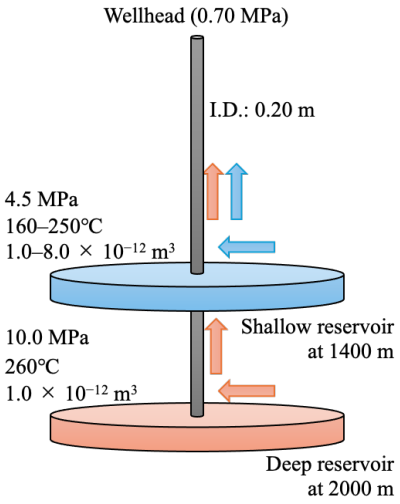

Figure 1: Schematic of the simulation model. The parameter values are for the reference case. The three variant cases assumed different wellbore inner diameter (0.14 m), wellhead pressure (0.30 MPa), and shallow reservoir pressure (5.0 MPa).

4. RESULTS AND DISCUSSIONS

4.1 Velocity profiles with the slip

First, we observed the velocity profiles along the wellbore to clarify the significance of slip. The initial distributions of the velocities of the liquid phase u_l, vapor phase u_v, and mixture u_{mix}, as well as the flowing mass fraction of the vapor phase (quality) x, for a run of the reference case are presented in Figure 2. The flow velocity of the mixture u_{mix}, simulated using the homogeneous flow model, is also superimposed for reference. The temperature and permeability–thickness product of the shallow reservoir are 230°C and 4×10^{-12} m^3, respectively. From the profile of x, we identified two flash points at depths of 1341 and 1472 m. The liquid-phase interval between these flash points was formed by the inflow of the low-enthalpy fluid into the shallow feed zone (1400 m). In the two-phase interval, the obvious differences between u_v and u_l indicate the significance of the slip. The slip ratio u_v/u_l increased up to 6.03 at the wellhead. The flow velocity of the mixture u_{mix} simulated using the slip model coincides with that obtained using the homogeneous flow model. This coincidence was due to the specific features of the homogenous flow model, in which the void fraction was computed using Smith's equation (Smith, 1969–70), as employed by Matsumoto et al. (2021) and in preceding studies.

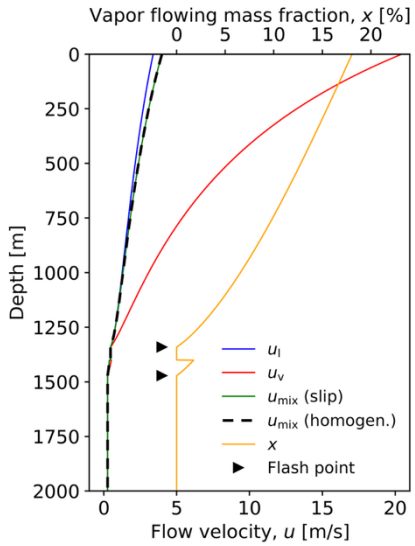

Figure 2: Profiles of flow velocities and flowing mass fraction of the vapor phase at the initiation of a run included in the reference case. The temperature and permeability–thickness product of the shallow reservoir are 230°C and 4×10^{-12} m^3, respectively. The static mean flow velocity u_{mix} simulated using the homogeneous flow model is superimposed.

4.2 Flow patterns

Next, we focused on a few runs of the reference case to observe the flow patterns in detail. Figures 3 and 4 show the temporal changes in the production rate (i.e., mass flow rate at the wellhead) simulated using the homogeneous flow and slip models, respectively. The simulations using the homogeneous flow model (Figure 3) are the same as those presented by Matsumoto et al. (2021; Figure 3). The permeability–thickness product of the shallow reservoir is commonly 4.0×10^{-12} m^3. The flow patterns were categorized into three groups: constant, periodic, and unstable flows. Constant and periodic flows are stably sustained with a constant or periodically changing production rate, whereas unstable flows cease irregularly. The irregular halts of the unstable flows are apparently due to numerical failures in solving the nonlinear system using the Newton–Raphson method, which implies that the conservation of mass, energy, and momentum is not sustainably satisfied under the given conditions.

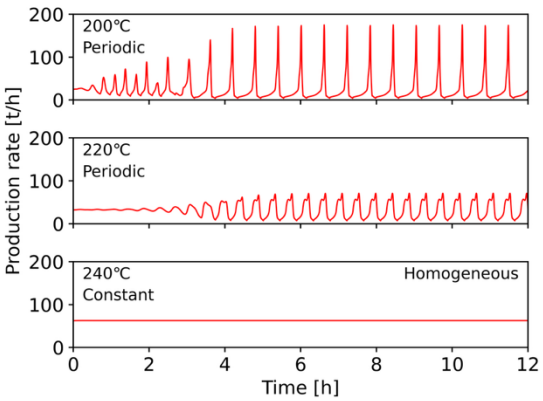

Figure 3: Temporal changes in the production rate simulated using the homogeneous flow model for three runs of the reference case. The permeability–thickness product of the shallow reservoir is 4×10^{-12} m^3.

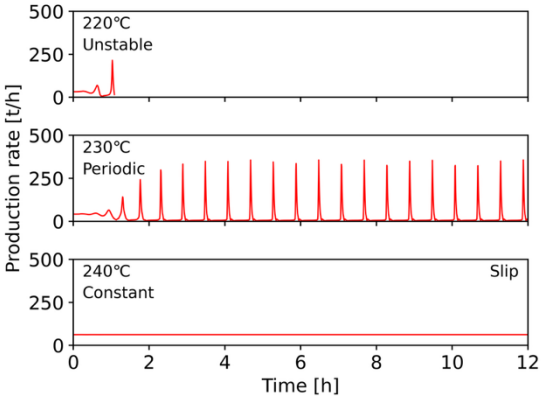

Figure 4: Temporal changes in the production rate simulated using the slip model for three runs included in the reference case. The permeability–thickness product of the shallow reservoir is 4×10^{-12} m^3. The initial state of the run for 230°C is presented in Figure 2.

The flow pattern transitioned from constant to unstable flows through periodic flows, with a decrease in the shallow reservoir temperature. Compared to the homogeneous flow model, the slip model exhibited periodic flows only within a relatively narrow temperature interval. In fact, the homogeneous flow model still sustained the periodic flow at a shallow reservoir temperature of 180°C. As Matsumoto et al. (2021) presented, periodicity is generated through the following steps:

1) The inflow of the low-enthalpy fluid into the shallow feed zone generates an interval filled with the liquid phase.

2) The existence of the liquid-phase interval above the shallow feed zone depth increases the shallow feed zone pressure owing to its weight and interruption of the upflow, causing a decline in the inflow of the low-enthalpy fluid.

3) The liquid-phase interval ascends toward the wellhead, followed by a relatively high-enthalpy fluid from the deep feed zone, and subsequently flashes, which generates a sharp peak in the production rate.

4) The ejection of a large portion of the fluid mass in the total wellbore rapidly decreases the shallow feed zone pressure, which resumes the inflow of the low-enthalpy fluid and generates another liquid-phase interval.

In the steps described above, the ascent of the liquid-phase interval, followed by its flash, is essential for stably sustaining the periodic flow. By allowing slip in the simulation model, the ascent of the liquid-phase interval severely declined, owing to the degradation of the holdup. Consequently, periodic flow was observed within a relatively narrow range of conditions.

4.3 Condition for generating periodicity

Finally, we discuss the variation in flow patterns with respect to the ratios of productivity indices and specific enthalpies between the shallow and deep reservoirs. The condition for generating periodicity (Equation 1), derived from numerical experiments using the homogeneous flow model, can be rewritten as follows:

$$1-\frac{h_{\mathrm{reS}}}{h_{\mathrm{reD}}}>\kappa\left(1-\frac{h_{\mathrm{L}}}{h_{\mathrm{reD}}}\right)\left(\frac{\mathrm{PI_S}}{\mathrm{PI_D}}\right)^{-1}+1-\frac{h_{\mathrm{L}}}{h_{\mathrm{reD}}}. \qquad (6)$$

This indicates that the boundary between the constant and periodic flows is depicted using a curve of inverse proportion in space, with coordinates $\mathrm{PI_S}/\mathrm{PI_D}$ and $1-h_{\mathrm{reS}}/h_{\mathrm{reD}}$ (or $h_{\mathrm{reS}}/h_{\mathrm{reD}}$ with an inverted axis). We particularly focus on the applicability of this condition to simulations using the slip model and the values of κ and $h_{\mathrm{reD}}/h_{\mathrm{L}}$ if applicable.

The flow patterns for 50 runs of the reference case are summarized in Figure 5. The curve obeying Equation 6 successfully divides the regions of constant and periodic flows. The value of the factor κ was empirically determined by adjusting to successfully divide the two regions. The value of h_{L}, which is the lower limit of the specific enthalpy of the deep reservoir h_{reD} for sustaining production without a shallow reservoir, was determined by performing steady-state simulations without a shallow reservoir, including trial-and-error modifications of h_{reD}. In comparison with the boundary determined using the homogeneous flow model (Matsumoto et al., 2021, Figure 8), κ had a smaller value, while h_{L} did not rely on the models. Consequently, the region containing periodic and unstable flows was expanded by replacing it with the slip model. The flow patterns for the 50 runs of each variant are shown in Figure 6. Similar to the reference case, the replacement with the slip model expanded the region of periodic/unstable flow with smaller values of κ, while h_{L} did not rely on the models. A large portion of the periodic flow runs became unstable when replaced with the slip model, which implied that the periodic flows could be stably sustained within a narrow temperature interval of the shallow reservoir, as discussed in Section 4.2.

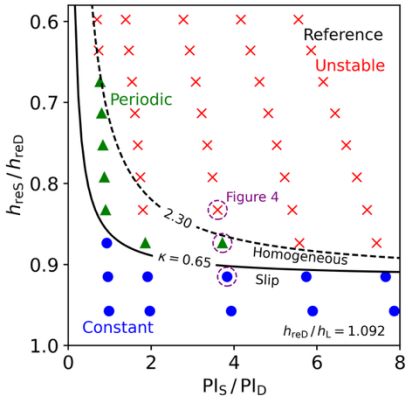

Figure 5: Flow patterns for the reference case, depending on the productivity index and specific enthalpy ratios between the shallow and deep reservoirs. The solid curve denotes the boundary between the constant and periodic flows based on Equation 6. The boundary denoted by the broken curve, determined using the homogeneous flow model, is superimposed for reference. The flow patterns for the three indicated runs are presented in Figure 4.

The empirical factor κ modifies the weight involved in the mean specific enthalpy defined in the right-hand side of Equation 1. The simulation results using the homogenous flow model exhibited the values of κ to be commonly larger than unity, which implied the excess impact of inflow at the deep feed zone beyond the magnitude of productivity indices. Matsumoto et al. (2021) concluded that this excess impact was caused by the asymmetrical condition between the fluids flowing in the wellbore, originating in the shallow and deep feed zones. The fluid from the shallow feed zone always shares a wellbore interval with that from the deep feed zone, whereas the fluid from the deep feed zone shares an interval only when flowing above the shallow feed zone (Figure 1). Sharing the wellbore interval prevents flows, including inflow at the feed zone. Under the same asymmetrical condition, the values of κ determined using the slip model are commonly smaller than those using the homogeneous flow model, and occasionally smaller than even unity. We interpret this feature as a significant effect of the slip between the liquid and vapor phases. As discussed in Section 4.2, the slip causes a severe decline in the ascent of the liquid-phase interval. The slip can also promote the formation of the liquid-phase interval by efficiently settling the liquid phase. This effect strengthens the impact of inflow at the shallow feed zone, reducing the value of κ.

The lower limit of the deep reservoir specific enthalpy, h_{L}, as well as the reservoir specific enthalpy normalized by this limit, $h_{\mathrm{reD}}/h_{\mathrm{L}}$, were not affected by the replacement of the two-phase flow model. This feature does not seem realistic because a significant slip degrades the holdup of the liquid phase and consequently halts wellbore flows. The value of h_{L} was theoretically determined by extrapolating a regression curve based on the production rates and deep reservoir specific enthalpies to determine the specific enthalpy at which the production rate was zero. From this theoretical perspective, without strictly simulating halts in production, the slip becomes insignificant as the production rate and flow velocities of both the phases approach zero. Therefore, the value of h_{L} does not depend on the two-phase flow model. The process of determining h_{L}, as described

above, should be noted when the applicability of the condition for generating periodicity (Equations 1 and 6) to actual wells is discussed in future studies.

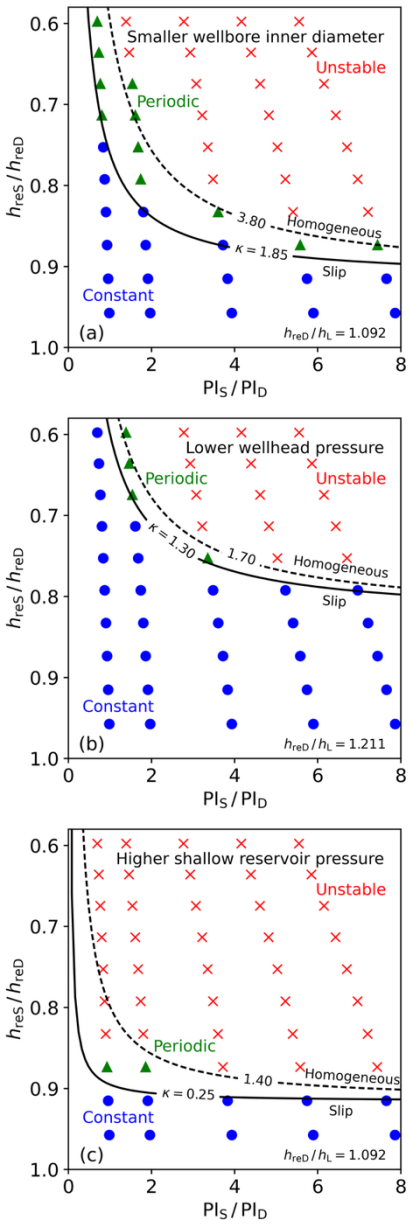

Figure 6: Flow patterns for the variant cases depending on the productivity index and specific enthalpy ratios between the shallow and deep reservoirs: (a) smaller wellbore inner diameter of 0.14 m, (b) lower wellhead pressure of 0.30 MPa, and (c) higher shallow reservoir pressure of 5.0 MPa. The solid and broken curves denote the boundaries between constant and periodic flows based on Equation 6, determined using the slip and homogeneous flow models.

5. CONCLUSION

We performed numerical experiments to partially validate the condition for generating periodic wellbore flow presented by Matsumoto et al. (2021), who assumed a vertical well intersecting shallow and deep reservoirs with different specific enthalpies and productivity indices. By replacing the original homogeneous flow model with the slip model, the effects of the slip between the liquid and vapor phases on the condition were investigated. From the results of the 200 numerical experiments, we conclude that:

1) The condition based on the mean specific enthalpy of shallow and deep reservoirs weighted by their productivity indices (Equations 1 and 6) is applicable to simulations using the slip model, which supports the generality of the condition and its applicability to actual wells.

2) Owing to the slip degrading the holdup of the liquid phase, stably periodic flows are generated within a narrow interval of the shallow reservoir temperature because the ascent of the liquid-phase interval, which is essential for generating periodic flows, significantly declines.

3) In addition to the decline of the ascending liquid-phase interval, the slip also promotes the formation of the liquid-phase interval by efficiently settling the liquid phase, which reduces the value of the empirical factor κ, occasionally below unity.

4) The lower limit of the deep reservoir specific enthalpy h_L does not depend on the two-phase flow models, regardless of the existence or absence of slip. It should be noted that h_L, determined theoretically, does not coincide with the limitations observed in actual wells.

These are expected to be validated in future studies using other sophisticated two-phase flow models (e.g., drift flux models) and by referring to actual wells.

ACKNOWLEDGEMENTS

This study was based on the results obtained from project JPNP21001 commissioned by the New Energy and Industrial Technology Development Organization (NEDO).

REFERENCES

Colebrook, C.F., (1939). Turbulent flow in pipes, with particular reference to the transition region between the smooth and rough pipe laws. *Journal of the Institution of Civil Engineers 11*, 133–156.

Grant, M.A., Bixley, P.F., Syms, M.C., (1979). Instability in well performance. *GRC Trans. 3*, 275–278.

Grant, M.A., Bixley, P.F., (2011). Geothermal reservoir engineering, second ed. Academic Press, Burlington.

Inagaki, H., Itoi, R., Kumagai, N., Iwasaki, T., (2014). Numerical simulation on fluctuation in wellhead pressure of geothermal well. *Proceedings, 39th Workshop on Geothermal Reservoir Engineering*.

Itoi, R., Katayama, Y., Tanaka, T., Kumagai, N., Iwasaki, T., (2013). Numerical simulation of instability of geothermal production well. *GRC Trans. 37*.

Itoi, R., Inagaki, H., Tanaka, T., Iwasaki, T., (2014). Effects of low temperature water inflow into wellbore at shallow feed zone of production well on steam-water two-phase flow in well. *Proceedings, 36th New Zealand Geothermal Workshop*.

Iwata, S., Nakano, Y., Granados, E., Butler, S., Robertson-Tait, A., (2002). Mitigation of cyclic production behavior in a geothermal well at the Uenotai geothermal field, Japan. *GRC Trans. 26*, 193–196.

Katayama, Y., Itoi, R., Kumagai, N., Iwasaki, T., (2011). Flow characteristics of geothermal production well with multi-feed zones. *GRC Trans. 35*, 1475–1479.

Katayama, Y., Itoi, R., Tanaka, T., (2013). Numerical simulation of transient two-phase flow in geothermal production well with multi-feed zones. *Proceedings, 2nd ITB Geothermal Workshop*.

Matsumoto, M., Itoi, R., Fujimitsu, Y., (2021). Theoretical study of conditions for generation of periodic wellbore flow due to inflow of a lower-enthalpy fluid. *Geothermics 89*, 101948.

Matsumoto, M., Okada, H., Itoi, R., Fujimitsu, Y., (2023). Numerical simulation of periodic wellbore flow due to the inflow of low-enthalpy fluid. *Proceedings, 48th Workshop on Geothermal Reservoir Engineering*.

Matus Pravia, I.A., Prado Reyes, L.L., Guidos Pineda, J.A., (2020). Case study: SJ9-3 fork leg cycling production well of the San Jacinto Tizate geothermal field, Nicaragua. *Proceedings, World Geothermal Congress 2020+1*.

Pan, L., Oldenburg, C.M., (2014). T2Well—An integrated wellbore–reservoir simulator. *Computers & Geosciences 65*, 46–55.

Smith, S.L., (1969–70). Void fractions in two-phase flow: A correlation based upon an equal velocity head model. *Proceedings, Instn. Mech. Engrs. 184*, *Pt 1*, *36*, 647–664.

Tonkin, R., O'Sullivan, M., O'Sullivan, J., (2021). A review of mathematical models for geothermal wellbore simulation. *Geothermics 97*, 102255.

Tonkin, R., O'Sullivan, J., Gravatt, M., O'Sullivan, M., (2023). A transient geothermal wellbore simulator. *Geothermics 110*, 102653.

Yamamura, K., Itoi, R., Tanaka, T., Iwasaki, T., (2016). Numerical model of transient steam-water two-phase flow in geothermal production wells. *Proceedings, 38th New Zealand Geothermal Workshop*.

Yamamura, K., Itoi, R., Tanaka, T., Iwasaki, T., (2017). Numerical analysis of transient steam-water two-phase flow in geothermal production wells with multiple feed zones. *Proceedings, 42nd Workshop on Geothermal Reservoir Engineering*.

ISSN 2703-4275